Katholieke Universiteit Leuven

Departement Elektrotechniek ESAT-SISTA/TR 2000-68

DFT Modulated Filter Bank Design for Oversampled Subband Systems [1]

Koen Eneman, Marc Moonen [2]

Published in Signal Processing vol. 81(9), pp. 1947-1973
September 2001

[1]This report is available by anonymous ftp from *ftp.esat.kuleuven.ac.be* in the directory *pub/SISTA/eneman/reports/00-68.ps.gz*

[2]ESAT (SISTA) - Katholieke Universiteit Leuven, Kasteelpark Arenberg 10, 3001 Leuven (Heverlee), Belgium, Tel. 32/16/321809, Fax 32/16/321970, WWW: *http://www.esat.kuleuven.ac.be/sista*. E-mail: *koen.eneman@esat.kuleuven.ac.be*. Marc Moonen is a Research Associate with the F.W.O. (Fund for Scientific Research – Flanders). This research work was carried out at the ESAT laboratory of the Katholieke Universiteit Leuven, in the frame of the Belgian State Interuniversity Poles of Attraction Programme – IUAP P4–02 (1997–2001) : Modeling, Identification, Simulation and Control of Complex Systems, Concerted Research Action GOA–MEFISTO–666 of the Flemish Government, Research Project F.W.O. nr. G.0295.97 ('Design and implementation of adaptive digital signal processing algorithms for broadband applications') and IWT project AUT/970517: MUSETTE ('Multimicrophone Signal Enhancement Techniques for handsfree telephony and voice controlled systems'). The scientific responsibility is assumed by its authors.

DFT Modulated Filter Bank Design for Oversampled Subband Systems

Koen Eneman Marc Moonen
ESAT – Katholieke Universiteit Leuven
Kardinaal Mercierlaan 94, B–3001 Heverlee – Belgium
phone : +32/16321809 +32/16321060
fax : +32/16321970
email : koen.eneman@esat.kuleuven.ac.be
marc.moonen@esat.kuleuven.ac.be

Abstract

Filter banks are widely used in digital signal processing, often integrated in a multirate scheme, to reduce the implementation cost and to improve algorithmic performance. DFT modulated filter banks are commonly used to design oversampled subband schemes. Oversampled subband schemes are attractive as they trade off between complexity gain and aliasing distortion. Ideally, the overall effect of a subband system is that of a pure delay, i.e. the subband system is perfectly reconstructing. In this paper we present design techniques for perfect and nearly perfect reconstruction oversampled DFT modulated filter banks. One of the disadvantages of perfect reconstruction filter bank design is that the stopband attenuation of the filters is typically small, which could have a negative impact on intermediate subband operations such as subband adaptive filtering. Nearly perfect reconstruction filter banks can be designed to overcome this problem, leading to a better performance of the intermediate algorithms.

1 Introduction

Filter banks are widely used in digital signal processing [10]. Typical applications are subband coding [7][12] and subband adaptive filtering [9][5]. Subband techniques can improve the performance of standard fullband algorithms for speech, audio or image processing as they provide an optimally tuned algorithm in each subband, outperforming the globally tuned fullband algorithm. Furthermore, by combining filter banks with multirate techniques the implementation cost can typically be reduced.
A general subband scheme is shown in figure 1. The so–called analysis filter bank splits the input x in a set of smallband signals. Hence, intermediate coding or adaptive filtering operations can be performed on the subband signals

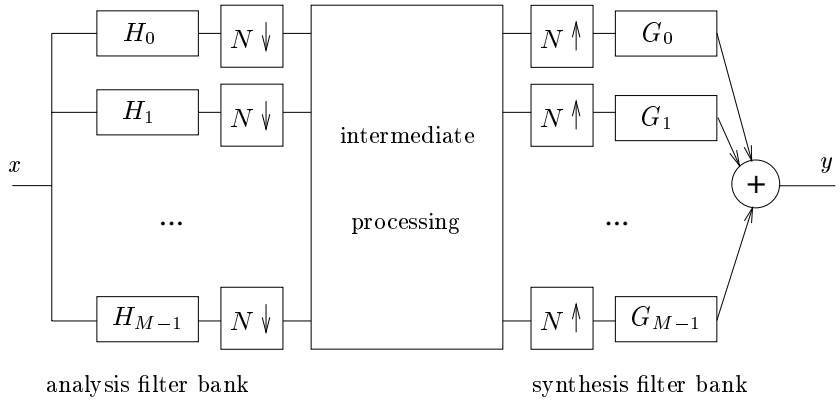

Figure 1: A general subband scheme : all intermediate operations can be done at the downsampled rate which typically leads to a reduced implementation cost and improved performance.

at the downsampled rate and this typically leads to a cheaper implementation. When modulated filter banks are used, one can rely on fast signal transforms and polyphase decomposition such that also the filter operations can be efficiently done at the downsampled rate [10].
The implementation cost can be optimally reduced when the subbands are maximally decimated (i.e. when $M = N$ in figure 1), but these critically downsampled subband schemes insert a considerable amount of aliasing in the subbands. Inter–subband aliasing often has an impeding effect on intermediate operations performed on the subband signals (e.g. subband adaptive filtering). From this point of view oversampled subband schemes ($M > N$) are more attractive as they trade off between complexity reduction and aliasing distortion.
Ideally, in the absence of intermediate processing, the overall effect of a subband system is equivalent to a pure delay, i.e. output y is a delayed copy of the input x (see figure 1). The design of critically downsampled DFT or DCT modulated filter banks having this perfect reconstruction property is well–known and leads to the design of para–unitary or unimodular polyphase matrices [10][13][14]. Some references on perfect reconstruction design for oversampled DFT modulated filter banks can be found in more recent publications such as [2][8][11]. In this paper a design technique for perfect and nearly perfect reconstruction oversampled DFT modulated filter banks will be presented.
In section 2 and 3 we will discuss some properties of oversampled filter banks. Section 4 derives the perfect reconstruction condition. In section 5 a design technique for perfect reconstruction oversampled DFT modulated filter banks will be presented. It will be shown that the stopband attenuation of these filter banks is typically small, which could have a negative impact on intermediate subband operations. In section 6 two design techniques for nearly perfect re-

construction oversampled DFT modulated filter banks will be presented. In the last section subband adaptive filtering is taken as an example to illustrate that thanks to their lower stopband level nearly perfect reconstruction filter banks can outperform perfect reconstruction systems.

2 Oversampled Filter Banks

2.1 Polyphase implementation

The analysis filter bank is immediately followed by downsamplers (see figure 1). Hence it is cheaper to also do the filter bank operations at the downsampled rate. Figure 1 can therefore be re–arranged, resulting in figure 2 (omitting the intermediate processing for a while). $\mathbf{H}(z)$ and $\mathbf{G}(z)$ are respectively called the

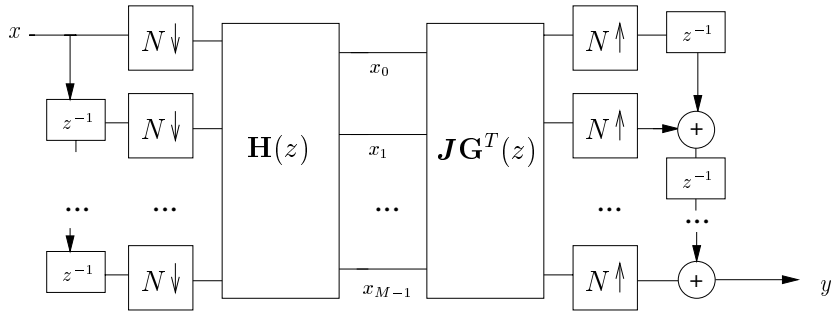

Figure 2: Oversampled subband system : polyphase implementation

analysis and synthesis polyphase matrix. Element (m, n) of $\mathbf{H}(z)$ is

$$[\mathbf{H}(z)]_{mn} = H_{m_{n:N}}(z) \qquad \begin{cases} m = 0 \to M-1 \\ n = 0 \to N-1 \end{cases} \tag{1}$$

$H_{m_{n:N}}(z)$ is the n–th out of N polyphase components of the m–th subband filter $h_m[k]$, in other words the z–transform of $h_m[n + Nk]$, $k = 0, 1, \ldots$. Similarly,

$$[\mathbf{G}(z)]_{mn} = G_{m_{n:N}}(z) \qquad \begin{cases} m = 0 \to M-1 \\ n = 0 \to N-1 \end{cases} \tag{2}$$

$\boldsymbol{J}$ is the exchange matrix with 1's along its main anti–diagonal and 0's elsewhere.

2.2 Modulated filter banks

Computationally efficient oversampled subband systems are often based on modulated filter banks, which typically use DCT or DFT operations [10].
The M subband filters of a DFT modulated filter bank are derived by frequency

shifting a well–designed prototype lowpass filter $h_0[k]$ of length L_a :

$$h_m[k] = h_0[k]e^{-j\frac{2\pi km}{M}}, \qquad \begin{cases} m = 0 \rightarrow M-1 \\ k = 0 \rightarrow L_a - 1 \end{cases} \tag{3}$$

$$\Leftrightarrow$$

$$H_m(z) = H_0(e^{j\frac{2\pi m}{M}}z) \tag{4}$$

The filters are frequency shifted versions of each other and the complete set of M filters covers the whole frequency spectrum.
Cosine or DCT modulated filter banks are a well–known alternative for DFT modulated filter banks and are often based on the QMF–principle [10]. Based on a well–designed FIR prototype filter $p[k]$ of length L_a the different DCT analysis filters $h_m[k]$ can be derived as follows [10] :

$$h_m[k] = 2p[k]\cos\left(\frac{\pi}{M}\left(m+\frac{1}{2}\right)\left(k-\frac{L_a-1}{2}\right)+(-1)^m\frac{\pi}{4}\right), \quad m = 0 \rightarrow M-1 \tag{5}$$

Whereas DCT modulated filter banks are typically used in critically downsampled subband systems, they are less suitable for oversampled schemes. Cosine modulated filters have a positive and negative frequency band. The positive and negative frequent subbands tend to overlap when the subband signals are downsampled and in this way aliasing is inserted in the subbands. As it is our goal to design true oversampled filter banks ($M > N$) which introduce a small amount of inter–subband aliasing, standard DCT modulated filter banks are not applicable. Some schemes have been proposed which combine real filter banks with unequal subsampling in different bands to overcome this problem [6].
In the case of DFT modulated filter banks the subband filters are complex–valued and filter out a single contingent frequency region. If there are M subbands and the prototype lowpass filter has a good stopband rejection, the bandwidth of the bandpassed signals which are filtered out by each of the subband filters is approximately $\frac{f_s}{M}$ such that during the downsampling process the subbands are correctly projected into the new fundamental interval $[\frac{-f_s}{2N}, \frac{f_s}{2N}]$, avoiding aliasing distortion. As a consequence oversampled subband schemes are often based on DFT modulated filter banks because of their aliasing robustness and ease of implementation.

3 Oversampled DFT Modulated Filter Banks

DFT modulated filter banks can be implemented efficiently using polyphase decomposition and fast signal transforms. In [2] a general framework for oversampled DFT modulated subband systems was proposed. It was proven that an M–band DFT modulated analysis filter bank with N–fold downsampling can be realised as a tapped delay line of size N followed by a structured $M \times N$ polynomial matrix $\mathbf{B}(z)$, containing polyphase components of the prototype h_0, and finally an $M \times M$ DFT matrix $\mathbf{F}$ (see figure 3). It can be shown [2][3] that

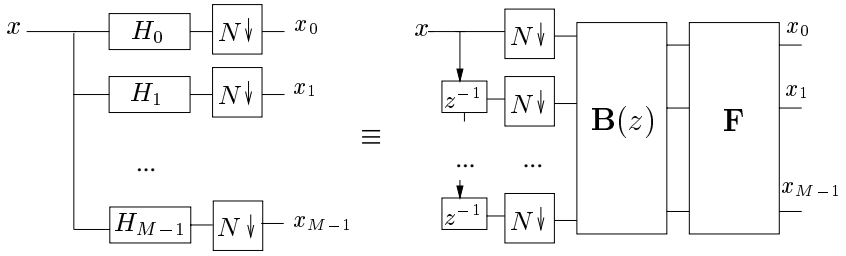

Figure 3: A DFT modulated analysis filter bank with M subbands followed by N–fold downsamplers. By employing FFT techniques ($\mathbf{F}$) and polyphase decomposition ($\mathbf{B}(z)$) an efficient implementation is feasible.

element (m, n) of $\mathbf{B}(z)$ is given by :

$$\begin{aligned} [\mathbf{B}(z)]_{mn} &= z^{-l} E_{(n+lN):K}(z^J) && \text{if } (m-n) \bmod g = 0 \\ &= 0 && \text{if } (m-n) \bmod g \neq 0 \end{aligned} \tag{6}$$

in which $0 \leqslant m < M$ and $0 \leqslant n < N$. Further, $(n + lN) \bmod M = m$, $g = \gcd(M, N)$, $J = \frac{M}{g}$ and $K = \frac{MN}{g}$. $E_{k:K}(z)$ is the k–th out of K polyphase components of the prototype filter h_0. Element (p, q) of $\mathbf{F}$ is given by $[\mathbf{F}]_{pq} = e^{-j\frac{2\pi pq}{M}}$.

Consider the following example : a DFT modulated subband system with 6 subbands ($M = 6$) and downsampling factor 4 ($N = 4$) is constructed. For this example $g = \gcd(6, 4) = 2$ and $K = \frac{6.4}{2} = 12$. Let $H_0(z)$ be the lowpass prototype filter and $E_{k:12}(z)$ the polyphase components of $H_0(z)$. Following Eq. 6 we obtain

$$\mathbf{B}(z) = \begin{bmatrix} E_{0:12}(z^3) & 0 & z^{-1}E_{6:12}(z^3) & 0 \\ 0 & E_{1:12}(z^3) & 0 & z^{-1}E_{7:12}(z^3) \\ z^{-2}E_{8:12}(z^3) & 0 & E_{2:12}(z^3) & 0 \\ 0 & z^{-2}E_{9:12}(z^3) & 0 & E_{3:12}(z^3) \\ z^{-1}E_{4:12}(z^3) & 0 & z^{-2}E_{10:12}(z^3) & 0 \\ 0 & z^{-1}E_{5:12}(z^3) & 0 & z^{-2}E_{11:12}(z^3) \end{bmatrix}. \tag{7}$$

The synthesis bank is constructed in a similar fashion with an $N \times M$ matrix $\mathbf{C}(z)$ as shown in figure 4.

By employing FFT techniques and a polyphase decomposition of the lowpass prototype an efficient implementation is feasible. For an FIR filter bank with filters of length L_a implemented in the standard way as in figure 1 the number of elementary filter operations[1] per second amounts to ML_af_s, where f_s is the sampling frequency of the input signal x. The number of elementary operations per second required to implement a DFT modulated filter bank in an efficient

[1] An elementary filter or *multiply–accumulate* operation can be efficiently computed on dedicated processors (DSPs) and counts for 1 machine cycle.

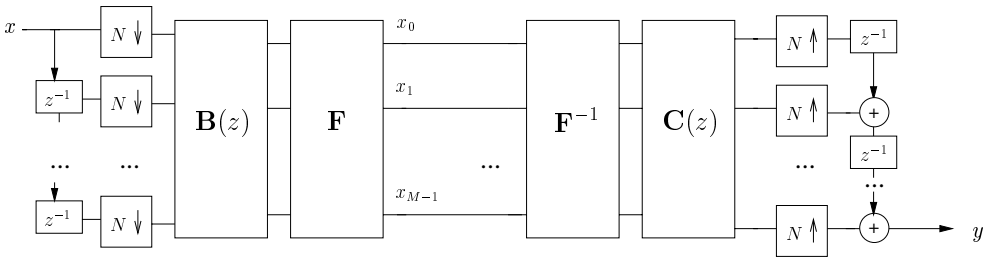

Figure 4: A DFT modulated subband system with polyphase decomposition for both the analysis and the synthesis filter bank.

way using FFT and polyphase decomposition is $(2M \log_2 M - 4M + 6)\frac{f_s}{N}$ for the FFT[2] plus $L_a \frac{f_s}{N}$ for the computation of $\mathbf{B}(z)$ as only K of the MN entries of $\mathbf{B}(z)$ are non–zero filters of length $\frac{L_a}{K}$. Instead of M filters in the standard approach, in this case only the equivalent of 1 filter is implemented together with an FFT, both at the downsampled rate.
For a realistic setup ($M = 16$, $N = 12$, $L_a = 48$ and $f_s = 8000$ Hz) the standard implementation would come down to 6144000 operations per second. For the efficient implementation this would reduce to 78667 operations per second. This proves that the cost reduction which can be achieved by efficiently implemented DFT modulated banks is considerable.

4 Perfect Reconstruction

Ideally, signal y at the output of the subband scheme (see figure 4) is an exact (delayed) copy of the input x. A DFT modulated analysis/synthesis filter bank set is therefore designed such that the following conditions are met :

- for the analysis/synthesis filter bank set the *perfect reconstruction* property holds. A condition ensuring perfect reconstruction is

$$\mathbf{C}(z)\mathbf{B}(z) = z^{-\delta}\mathbf{I}_N, \qquad \delta \in \mathbb{N}. \tag{8}$$

  In this case the inner filter operations (see figure 4) cancel each other out and the subband scheme reduces to a combined analysis and synthesis tapped delay line. It can be verified that this leads to perfect reconstruction. The smallest δ is determined such that Eq. 8 is fulfilled and such that both the analysis and synthesis filters are causal and hence implementable. Condition 8 can be relaxed to

$$\mathbf{C}(z)\mathbf{B}(z) \approx z^{-\delta}\mathbf{I}_N, \qquad \delta \in \mathbb{N} \tag{9}$$

[2] assuming that the input signal x is real.

leading to *nearly perfect reconstruction* up to a delay.
In a practical design δ is initially set equal to zero. This in general leads to non–causal filters, which can be compensated for after the design is completed.

- the (analysis) filters are *frequency selective*. This reduces the amount of aliasing components inserted in the subbands. Inter–subband aliasing often has a negative impact on possible intermediate operations performed on the subband signals (e.g. subband adaptive filtering). Highly frequency selective filter banks on the other hand are expensive and introduce a substantial processing delay. This puts a constraint on the frequency selectivity, and hence on the downsampling factor N. However, computational savings are more or less proportional to N.

In order to fulfil Eq. 8, $\mathbf{C}(z)$ has to be a left inverse of $\mathbf{B}(z)$. This left inverse exists if $M \geqslant N$. However, the synthesis filter bank which is obtained by inversion is not necessarily FIR or DFT modulated. In the most general case $\mathbf{C}(z)$ is a dense rational matrix and hence, the corresponding filter bank is IIR. Assume that the Smith–McMillan decomposition of the polynomial matrix $\mathbf{B}(z)$ is given by (see [10])

$$\mathbf{B}(z) = \mathbf{R}(z)\mathbf{D}(z)\mathbf{T}(z) \tag{10}$$

where $\mathbf{R}(z)$ and $\mathbf{T}(z)$ are respectively $M \times M$ and $N \times N$ unimodular matrices. This implies that their determinant is a non–zero constant or equivalently, that they can be decomposed as a product of elementary matrices [10]. $\mathbf{D}(z)$ is an $M \times N$ pseudo–diagonal matrix which can be expressed as

$$\mathbf{D}(z) = \begin{bmatrix} \mathbf{D}_1(z) \\ \mathbf{0}_{(M-N)\times N} \end{bmatrix} = \begin{bmatrix} d_1(z) & & \\ & \ddots & \\ & & d_N(z) \\ \mathbf{0}_{(M-N)\times N} & & \end{bmatrix}. \tag{11}$$

The synthesis bank $\mathbf{C}(z)$ which can be combined with $\mathbf{B}(z)$ to ensure perfect reconstruction, is

$$\begin{aligned} \mathbf{C}(z) &= \mathbf{B}^{\dagger}(z) + \mathbf{N}(z) && (12) \\ &= \mathbf{T}^{-1}(z)\left(\begin{bmatrix}\mathbf{D}_1^{-1}(z) & \mathbf{0}_{N\times(M-N)}\end{bmatrix} + \begin{bmatrix}\mathbf{0}_{N\times N} & \mathbf{X}(z)\end{bmatrix}\right)\mathbf{R}^{-1}(z). && (13) \end{aligned}$$

$\mathbf{N}(z)$ is an $N \times M$ matrix which lies in the left null space of $\mathbf{B}(z)$. $\mathbf{X}(z)$ is an $N \times (M-N)$ random rational matrix. $\mathbf{R}(z)$ and $\mathbf{T}(z)$ are unimodular polynomial matrices, so their inverse $\mathbf{R}^{-1}(z) = \mathrm{adj}\mathbf{R}(z)/\mathrm{det}\mathbf{R}(z)$ is also polynomial.
In the most general case $\mathbf{D}_1^{-1}(z)$ is rational and hence the synthesis filter bank is IIR. A true FIR inverse can be obtained if $\mathbf{D}_1(z)$ has monomial diagonal elements and $\mathbf{N}(z)$ is polynomial.
In order to obtain a modulated synthesis bank $\mathbf{C}(z)$ should be a polynomial matrix, with a structure analogue to that of $\mathbf{B}(z)$ (see Eq. 6). In this case the synthesis filters have equal spectral characteristics, up to a frequency shift.

Furthermore, a cheap implementation would be possible thanks to the special, sparse structure of $\mathbf{C}(z)$ (cf. Eq. 6). It appears that the inverse row and column operations $\mathbf{T}^{-1}(z)$ and $\mathbf{R}^{-1}(z)$ which act on $\begin{bmatrix}\mathbf{D}_1^{-1}(z) & \mathbf{0}\end{bmatrix}$ put $\mathbf{B}^\dagger(z)$ in the desired format i.e. a structure analogue to that of $\mathbf{B}(z)$. If $\mathbf{N}(z)$, based on a random $\mathbf{X}(z)$, is added to $\mathbf{B}^\dagger(z)$ the structure will not be maintained in general.
An elegant solution results when $\mathbf{X}(z) = \mathbf{0}$, $\mathbf{D}_1(z)$ and $\mathbf{T}(z)$ are chosen to be unit matrices and $\mathbf{R}(z)$ is para–unitary, i.e.

$$\tilde{\mathbf{R}}(z)\mathbf{R}(z) = \mathbf{I}_M, \qquad \mathbf{D}_1(z) = \mathbf{T}(z) = \mathbf{I}_N, \quad \mathbf{X}(z) = \mathbf{0}. \tag{14}$$

The paraconjugate of $\mathbf{R}(z)$, $\tilde{\mathbf{R}}(z) = \mathbf{R}_*^T(z^{-1})$, is obtained by transposing $\mathbf{R}(z)$, replacing all filter coefficients by their complex conjugate and replacing z by z^{-1} (see [10]). Hence,

$$\tilde{\mathbf{B}}(z)\mathbf{B}(z) = \mathbf{I}_N. \tag{15}$$

In this case $\mathbf{C}(z)$ can be chosen to be the paraconjugate of $\mathbf{B}(z)$:

$$\mathbf{C}(z) = \tilde{\mathbf{B}}(z). \tag{16}$$

Now,

$$\mathbf{C}(z)\mathbf{B}(z) = \tilde{\mathbf{B}}(z)\mathbf{B}(z) = \mathbf{I}_N, \tag{17}$$

so that a perfect reconstruction subband system is obtained. In this case $\mathbf{C}(z)$ is a polynomial matrix having a sparse structure, similar to the structure of $\mathbf{B}(z)$ (cf. Eq. 6). The synthesis polyphase matrix can be computed based on figure 2 and 4 and Eq. 16 :

$$\boldsymbol{J}\mathbf{G}^T(z) = \mathbf{C}(z)\mathbf{F}^{-1} \tag{18}$$

so that

$$\mathbf{G}^T(z) = \boldsymbol{J}\tilde{\mathbf{B}}(z)\mathbf{F}^{-1}. \tag{19}$$

Further, as the analysis polyphase matrix can be expressed as

$$\mathbf{H}(z) = \mathbf{F}\mathbf{B}(z) \tag{20}$$

we finally obtain

$$\mathbf{G}(z) = \frac{1}{M}\mathbf{H}_*(z^{-1})\boldsymbol{J}. \tag{21}$$

The synthesis filter bank is made causal, such that[3] (cf. Eq. 1, 2 and 3) :

$$g_m[k] = \frac{1}{M}\mathrm{conj}(h_m[L_a - 1 - k]) \tag{22}$$

$$= \frac{1}{M}e^{j\frac{2\pi(L_a-1)m}{M}}h_0[L_a - 1 - k]e^{-j\frac{2\pi km}{M}}. \tag{23}$$

It appears that the synthesis filter bank is a kind of modified oversampled DFT modulated filter bank. The synthesis filters $g_m[k]$ are shifted versions of each other and have the same frequency characteristics as the analysis filters.

[3] L_a is the length of $h_m[k]$.

5 Para–Unitary Oversampled Filter Bank Design

If $\mathbf{B}(z)$ can be made para–unitary as in Eq. 15 having the special format specified in Eq. 6, an oversampled DFT modulated perfect reconstruction filter bank set is straightforwardly obtained from Eq. 16 or 22.

5.1 Imposing para–unitariness

$\mathbf{B}(z)$ is a structured $M \times N$ matrix with non–zero entries in a specific pattern (e.g. Eq. 7). After appropriate row and column permutations $\mathbf{P}$ and $\mathbf{Q}$ a block diagonal matrix

$$\mathbf{PB}(z)\mathbf{Q} = \begin{bmatrix} \mathbf{S}_0(z) & \dots & \mathbf{0} \\ \vdots & \ddots & \vdots \\ \mathbf{0} & \dots & \mathbf{S}_{g-1}(z) \end{bmatrix} \tag{24}$$

can be obtained consisting of g dense sub–matrices $\mathbf{S}_\gamma(z)$ of dimension $\frac{M}{g} \times \frac{N}{g}$ [4][11]. As already defined in Eq. 6, g is the greatest common divisor of M and N. Further, γ is an integer between 0 and $g-1$. Referring to the example (Eq. 7), $\mathbf{B}(z)$ can be transformed into the following block diagonal matrix :

$$\mathbf{PB}(z)\mathbf{Q} = \left[\begin{array}{cc|cc} E_{0:12}(z^3) & z^{-1}E_{6:12}(z^3) & 0 & 0 \\ z^{-2}E_{8:12}(z^3) & E_{2:12}(z^3) & 0 & 0 \\ z^{-1}E_{4:12}(z^3) & z^{-2}E_{10:12}(z^3) & 0 & 0 \\ \hline 0 & 0 & E_{1:12}(z^3) & z^{-1}E_{7:12}(z^3) \\ 0 & 0 & z^{-2}E_{9:12}(z^3) & E_{3:12}(z^3) \\ 0 & 0 & z^{-1}E_{5:12}(z^3) & z^{-2}E_{11:12}(z^3) \end{array}\right]. \tag{25}$$

All $\frac{MN}{g}$ polyphase components of $h_0[k]$ are now contained in one of these sub–matrices. Note that the left and right multiplication with permutation matrices $\mathbf{P}$ and $\mathbf{Q}$ does not affect the para–unitariness of $\mathbf{B}(z)$ as for a permutation matrix $\mathbf{P}^T\mathbf{P} = \mathbf{I}$. Further, block diagonal matrix $\mathbf{PB}(z)\mathbf{Q}$ is para–unitary if each sub–matrix $\mathbf{S}_\gamma(z)$ itself is para–unitary. Hence, if we can find a set of para–unitary matrices $\mathbf{S}_\gamma(z)$ also $\mathbf{PB}(z)\mathbf{Q}$ and $\mathbf{B}(z)$ will be para–unitary.
It appears that the non–zero elements of $\mathbf{PB}(z)\mathbf{Q}$, namely $z^{-l}E_{(n+lN):K}(z^J)$ (cf. Eq. 6), are delayed J–fold upsampled polyphase filters. In practice $E_{(n+lN):K}(z)$ are optimised instead of their upsampled form. At first sight, the delays z^{-l} pose a problem : they cannot simply be downsampled as they are not powers of z^J. Now, it appears that the delays can always be made multiples of J by pre– and post–multiplication with appropriate para–unitary diagonal matrices $\mathbf{L}(z)$ and $\mathbf{R}(z)$. In this way all the elements of

$$\hat{\mathbf{S}}_\gamma(z^J) = \mathbf{L}(z)\mathbf{S}_\gamma(z)\mathbf{R}(z) \tag{26}$$

depend on z^J [3][11].
Again we take up the example : the sub–matrices $\mathbf{S}_\gamma(z)$ have dimensions 3×2.

After pre– and post–multiplication $\mathbf{S}_0(z)$ for instance looks like

$$\hat{\mathbf{S}}_0(z^3) = \underbrace{\begin{bmatrix} z & 0 & 0 \\ 0 & 1 & 0 \\ 0 & 0 & z^2 \end{bmatrix}}_{\mathbf{L}(z)} \mathbf{S}_0(z) \underbrace{\begin{bmatrix} z^{-1} & 0 \\ 0 & 1 \end{bmatrix}}_{\mathbf{R}(z)} = \begin{bmatrix} E_{0:12}(z^3) & E_{6:12}(z^3) \\ z^{-3}E_{8:12}(z^3) & E_{2:12}(z^3) \\ E_{4:12}(z^3) & E_{10:12}(z^3) \end{bmatrix}. \quad (27)$$

In conclusion, designing a para–unitary $\mathbf{B}(z)$ comes down to imposing para–unitariness on a set of dense matrices $\hat{\mathbf{S}}_\gamma(z)$.
Each of these rectangular blocks $\hat{\mathbf{S}}_\gamma(z)$ of size $\frac{M}{g} \times \frac{N}{g}$ can now be embedded in a larger square para–unitary matrix $\mathbf{M}_\gamma(z)$ of size $\frac{M}{g} \times \frac{M}{g}$ whose para–unitariness automatically implies the para–unitariness of a subset of its columns.

5.2 Para–unitary lattices

Square matrices can be parametrised to be para–unitary using para–unitary lattices. A causal real–valued $\frac{M}{g} \times \frac{M}{g}$ FIR para–unitary matrix of degree L can be decomposed as [10]

$$\mathbf{M}_\gamma(z) = \mathbf{V}_L(z)\mathbf{V}_{L-1}(z)\ldots\mathbf{V}_1(z)\mathbf{U} \quad (28)$$

where $\mathbf{V}_i(z)$ are degree–1 para–unitary building blocks (Householder type)

$$\mathbf{V}_i(z) = \mathbf{I}_{M/g} - \mathbf{v}_i\mathbf{v}_i^T + z^{-1}\mathbf{v}_i\mathbf{v}_i^T. \quad (29)$$

$\mathbf{U}$ is an orthonormal matrix which itself can be decomposed as

$$\mathbf{U} = \mathbf{U}_1\mathbf{U}_2\ldots\mathbf{U}_{M/g-1}. \quad (30)$$

in which $\mathbf{U}_i$ are Householder matrices

$$\mathbf{U}_i = \mathbf{I}_{M/g} - 2\mathbf{u}_i\mathbf{u}_i^T. \quad (31)$$

All $\mathbf{v}_i$ and $\mathbf{u}_i$ are $\frac{M}{g} \times 1$ unit norm vectors.
The $\frac{M}{g} \times \frac{M}{g}$ orthonormal matrix $\mathbf{U}$ is characterised by the $\frac{M}{g} - 1$ vectors $\mathbf{u}_i$. It can be proven (see [10]) that without loss of generality the description matrix $\begin{bmatrix} \mathbf{u}_1 & \mathbf{u}_2 & \ldots & \mathbf{u}_{M/g-1} \end{bmatrix}$ can have the following lower triangular form :

$$\begin{bmatrix} u_1(1) & 0 & \ldots & 0 \\ u_1(2) & u_2(2) & \ldots & 0 \\ \vdots & \vdots & \ddots & \vdots \\ u_1(\frac{M}{g}-1) & u_2(\frac{M}{g}-1) & \ldots & u_{M/g-1}(\frac{M}{g}-1) \\ u_1(\frac{M}{g}) & u_2(\frac{M}{g}) & \ldots & u_{M/g-1}(\frac{M}{g}) \end{bmatrix}. \quad (32)$$

5.3 Optimisation of the para–unitary lattices

A total of g square $\frac{M}{g} \times \frac{M}{g}$ matrices $\mathbf{M}_\gamma(z)$ are parametrised as in Eq. 28 to guarantee their para–unitariness, from which then automatically follows the para–unitariness of the $\frac{M}{g} \times \frac{N}{g}$ submatrices $\hat{\mathbf{S}}_\gamma(z)$. The analysis prototype filter $h_0[k]$ can be easily computed based on the parameter sets $(\mathbf{v}_i, \mathbf{u}_i)_\gamma$, parametrising each of the g para–unitary lattices : from $(\mathbf{v}_i, \mathbf{u}_i)_\gamma$ $\mathbf{M}_\gamma(z)$ and $\hat{\mathbf{S}}_\gamma(z)$ can be reconstructed following Eq. 28–30. $\hat{\mathbf{S}}_\gamma(z)$ determines the polyphase components of the analysis prototype $z^{-l}E_{(n+lN):K}(z^J)$ and hence $\mathbf{B}(z)$ can be obtained, from which immediately follows the filter bank characteristic. The parameter sets $(\mathbf{v}_i, \mathbf{u}_i)_\gamma$ are optimised such that the para–unitary filter bank has a good frequency selectivity and aliasing insertion due to the subsampling process is minimal. The stopband energy of the analysis prototype is therefore computed and minimised by a steepest descent optimisation procedure.
The delays present in $\hat{\mathbf{S}}_\gamma(z)$ (cf. Eq. 27) have to be taken in account when the elements of $\hat{\mathbf{S}}_\gamma(z)$ are linked to the prototype $h_0[k]$. The delays force the polyphase components to be shifted into the anti–causal direction. Although the number of non–zero coefficients is not affected by this, the length of the prototype increases. As a consequence, some of the coefficients of $h_0[k]$ will typically be zero. The number of operations needed to implement the filter remains unchanged, but the required amount of storage elements typically increases.
Finding a good initialisation for $\mathbf{v}_i$ and $\mathbf{u}_i$ is not trivial : the time needed to find a good lowpass prototype $h_0[k]$ depends on the quality of the initial values. Furthermore, the optimisation function (stopband energy) to be minimised is not unimodal and hence multiple local minima might exist. However, random initialisation will typically lead to satisfactory results after some trial rounds. Another option is to start from a well–chosen lowpass filter, obtained from a FIR filter design toolbox, and derive the $\mathbf{v}_i$ and $\mathbf{u}_i$ parameters corresponding to it. In general this will not be possible as a randomly designed lowpass filter will not lead to a para–unitary filter bank and hence a $(\mathbf{v}_i, \mathbf{u}_i)_\gamma$–parametrisation does not exist. However, the well–chosen prototype will be approximated by its "nearest" para–unitary filter, typically leading to better starting values. The $(\mathbf{v}_i, \mathbf{u}_i)_\gamma$–parametrisation of a para–unitary prototype can be found by inverse decomposition of Eq. 28 and 30. This can be done using the singular value decomposition, pseudo–inverses and Householder factorisation (see appendix A). For the special case of 2–fold oversampling ($M = 2N$) a more dedicated parametrisation is possible, which is based on 2–channel lossless lattices. In this case the so–called lattice rotation angles are optimised in order to obtain good lowpass characteristics. For more information, we refer to [3].

5.4 Adjusting the prototype filter length

L, the order of the para–unitary lattices (see Eq. 28) can be chosen freely and defines the length of the analysis prototype filter and hence the order of the filter bank. If the order of one of the para–unitary lattices is augmented from L to $L+1$, each of the $\frac{MN}{g^2}$ polyphase filters, defined by that specific lattice, becomes

longer and hence the analysis prototype gets an extra $\frac{MN}{g^2}$ coefficients. As a consequence at first sight, the number of effective (i.e. non–zero) coefficients of the prototype $h_0[k]$ can only vary in steps of $\frac{MN}{g^2}$. This can be unattractive for some coprime parameter settings. For example if $M = 16$ and $N = 15$, one has $g = 1$ and $\frac{MN}{g^2} = 240$. The higher the greatest common divisor of M and N, the more para–unitary lattices are involved and the better the length of the prototype can be adjusted. The minimal number of effective filter coefficients is obtained when all lattices have order 0. In that case all lattices $\mathbf{M}_\gamma(z) = \mathbf{U}_\gamma$ would be orthonormal matrices and the number of non–zero coefficients of $h_0[k]$ amounts to $\frac{MN}{g}$, which still can be quite large. However, with a special choice for $\mathbf{U}_\gamma$, the identity matrix for instance, the number of effective coefficients can be further reduced.
More generally, each of the g para–unitary lattices can be restricted to be a block diagonal matrix

$$\mathbf{M}_\gamma(z) = \begin{bmatrix} \mathbf{M}_{\gamma,0}(z) & \dots & \mathbf{0} \\ \vdots & \ddots & \vdots \\ \mathbf{0} & \dots & \mathbf{M}_{\gamma,R_\gamma-1}(z) \end{bmatrix}. \tag{33}$$

Each of the R_γ square blocks $\mathbf{M}_{\gamma,r}(z)$ is an $N_{\gamma,r} \times N_{\gamma,r}$ matrix such that

$$\sum_{r=0}^{R_\gamma-1} N_{\gamma,r} = \frac{M}{g}, \tag{34}$$

the size of $\mathbf{M}_\gamma(z)$. If now all $\mathbf{M}_{\gamma,r}(z)$ are parametrised as in Eq. 28 and 30 with unit–norm vectors $\mathbf{v}_i$ and $\mathbf{u}_i$ to guarantee that $\tilde{\mathbf{M}}_{\gamma,r}(z)\mathbf{M}_{\gamma,r}(z) = \mathbf{I}_{N_{\gamma,r}}$, also $\mathbf{M}_\gamma(z)$ and $\hat{\mathbf{S}}_\gamma(z)$ will be para–unitary. Depending on the block partitioning $N_{\gamma,r}$ and the order $L_{\gamma,r}$ of each of the blocks $\mathbf{M}_{\gamma,r}(z)$, some of the coefficients of $h_0[k]$ can be forced to be 0. In this way the effective length, i.e. the number of non–zero coefficients of $h_0[k]$ can be chosen more precisely and is not forced to vary in steps of $\frac{MN}{g^2}$.
Two special cases may be considered. If $N_{\gamma,r} > 1$ and $L_{\gamma,r} = 0$, $\mathbf{M}_{\gamma,r}(z) = \mathbf{U}$ is an orthonormal matrix. If $N_{\gamma,r} = 1$, only one coefficient can be different from 0 as $\tilde{\mathbf{M}}_{\gamma,r}(z)\mathbf{M}_{\gamma,r}(z) = 1$. Hence,

$$\mathbf{M}_{\gamma,r}(z) = z^{-L_{\gamma,r}}. \tag{35}$$

It is best to choose the lowest order and take $L_{\gamma,r} = 0$. If $N_{\gamma,r} = 1$ no optimisation can be done as the corresponding coefficient of $h_0[k]$ is restricted to be 1. In figure 5 a typical block partitioning is shown for a DFT modulated subband system with 6 subbands ($M = 6$) and downsampling factor 5 ($N = 5$) . $\mathbf{M}_\gamma(z)$ is a block diagonal matrix with $R_\gamma = 3$ blocks of length $N_{\gamma,0} = 3$, $N_{\gamma,1} = 1$ and $N_{\gamma,2} = 2$.
Given the $N_{\gamma,r}$ and $L_{\gamma,r}$ for all lattices and all blocks, and keeping in mind that only the first $\frac{N}{g}$ columns of $\mathbf{M}_\gamma(z)$ define $h_0[k]$, the effective length of $h_0[k]$ can

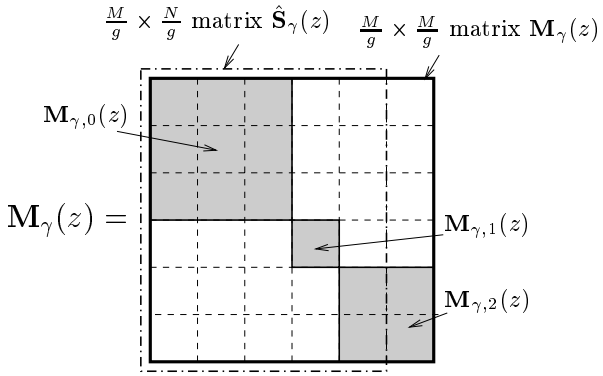

Figure 5: Typical block partitioning of $\mathbf{M}_\gamma(z)$ for $M = 6$ and $N = 5$.

be computed and is

$$L_{\text{ef}} = \sum_{\gamma=0}^{g-1} \left(N_{\gamma,\bar{R}_\gamma} Q_\gamma (L_{\gamma,\bar{R}_\gamma} + 1) + \sum_{r=0}^{\bar{R}_\gamma - 1} N_{\gamma,r}^2 (L_{\gamma,r} + 1) \right) \tag{36}$$

in which

$$Q_\gamma = \frac{N}{g} - \sum_{r=0}^{\bar{R}_\gamma - 1} N_{\gamma,r} \tag{37}$$

and $\bar{R}_\gamma$ is such that

$$\sum_{r=0}^{\bar{R}_\gamma - 1} N_{\gamma,r} < \frac{N}{g} \leqslant \sum_{r=0}^{\bar{R}_\gamma} N_{\gamma,r}. \tag{38}$$

Consider again the example of figure 5. It can be verified that $\bar{R}_\gamma = 2$, $N_{\gamma,\bar{R}_\gamma} = 2$ and $Q_\gamma = 1$.
Basically all effective filter lengths L_{ef} can be obtained with N being the minimum. This minimum is reached when all $\mathbf{M}_\gamma(z)$ are equal to the identity matrix. In the case of subband oversampling L_{ef} can be changed in steps of 2, starting from this minimum N, as for $M > N$

$$1 \leqslant \frac{N}{g} < \frac{M}{g}. \tag{39}$$

Hence, we can always find a block partitioning $N_{\gamma,r}$ for which $N_{\gamma,\bar{R}_\gamma} = 2$ and $Q_\gamma = 1$ such that L_{ef} changes in steps of $N_{\gamma,\bar{R}_\gamma} Q_\gamma = 2$ (see Eq. 36). The effective filter length can be further refined using 1×1 para–unitary blocks as a 1×1 block defines 1 coefficient, however restricted to 1. For the special case of critical downsampling ($M = N$), there are M para–unitary blocks $\mathbf{M}_\gamma(z)$ of size 1×1. As a consequence the prototype filter will consist of M filter coefficients equal to 1 (cf. Eq. 35).

Finding the optimal block partitioning $N_{\gamma,r}$ and block orders $L_{\gamma,r}$ in order to obtain a subband system with a desired effective filter length L_{ef} requires a rather computational intensive search over all possibilities. Typically, there exist multiple settings $(N_{\gamma,r}, L_{\gamma,r})$ leading to the same L_{ef}. The optimal partitioning should be found that minimises the number of coefficients forced to 0. Although the number of operations required to implement the filter bank is only determined by the effective length L_{ef}, the number of coefficients forced to 0 should be kept as small as possible. The larger this number, the more memory is required to implement the filter bank.
Furthermore, a large number of inserted zeros or ones restricts the design freedom and makes the optimisation of the para–unitary lattices harder. It will in general be more difficult to obtain a good lowpass frequency characteristic and an acceptable stopband level for the filter bank prototype when the number of inserted zeros and ones is large as these filter coefficients are fixed and cannot be changed by the optimisation procedure. Nearly perfect reconstruction filter banks (see section 6) may be employed to overcome this problem.

5.5 Design example

The above procedure for designing perfect reconstruction DFT modulated filter banks is illustrated by means of an example. Again the $M = 6$, $N = 4$ case is considered (cf. Eq. 7, 25 and 27). As $g = \gcd(6, 4) = 2$, there are 2 para–unitary matrices $\mathbf{M}_0(z)$ and $\mathbf{M}_1(z)$ of size 3×3 to be optimised (cf. section 5.2). In this example $\mathbf{M}_0(z)$ and $\mathbf{M}_1(z)$ were not further split up into block diagonal matrices and hence $R_0 = R_1 = 1$ and $N_{0,0} = N_{1,0} = 3$ (see section 5.4 for notation). Both $\mathbf{M}_0(z)$ and $\mathbf{M}_1(z)$ were chosen to be of second order, i.e. $L_{0,0} = L_{1,0} = 2$. As a consequence, the length of the prototype L_a is 40 and 36 taps appear to be non–zero as can be verified using Eq. 36. After running the optimisation procedure a lowpass FIR prototype filter $h_0[k]$ was obtained. The frequency response of the analysis prototype $H_0(f)$ is shown in figure 6. The relative aliasing level η introduced by a single filter bank

$$\eta = \sqrt{\frac{\int_{\frac{1}{2N}}^{\frac{1}{2}} |H_0(f)|^2 \, df}{\int_0^{\frac{1}{2N}} |H_0(f)|^2 \, df}} \tag{40}$$

is -37.7 dB. The characteristics of the synthesis prototype filter $g_0[k] = \frac{1}{M} h_0[L_a - 1 - k]$ are similar. By optimising the parameters $\mathbf{v}_i$ and $\mathbf{u}_i$ following the design procedure of section 5 the parameter set apparently converges to a para–unitary filter bank set with a relatively good frequency characteristic. As $R_0 = R_1 = 1$ in this example the number of zero coefficients is small. Hence, a fairly good frequency response could be obtained. However, for some applications the stopband energy remains too high. Nearly perfect reconstruction filter banks may be employed to overcome this problem. Furthermore, when a different block partitioning $N_{\gamma,r}$ is chosen with more inserted zeros nearly perfect reconstruction filter banks will easily outperform the perfect reconstruction filter bank in

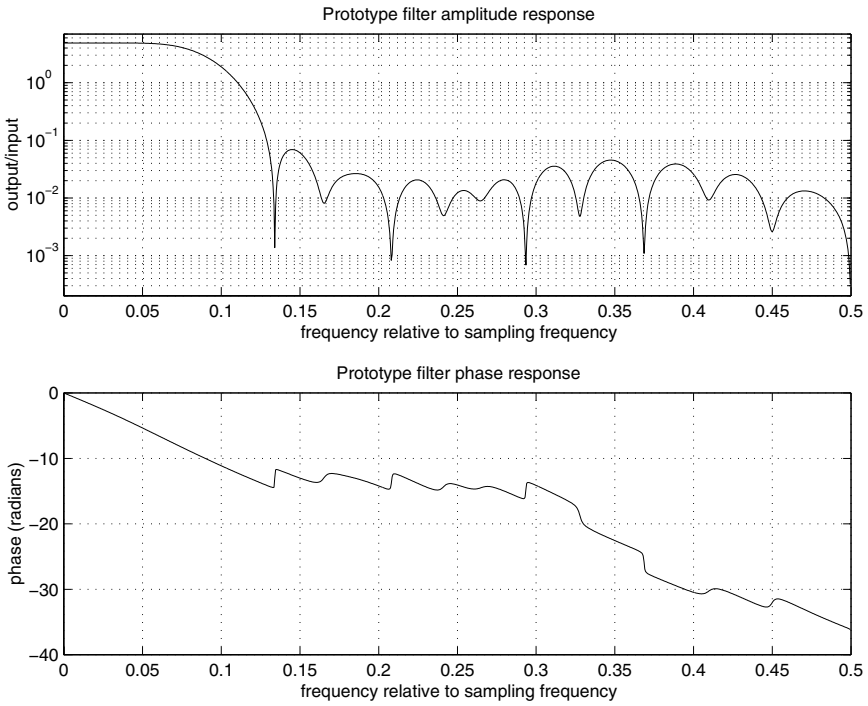

Figure 6: Perfect reconstruction oversampled filter bank : prototype frequency characteristic

terms of subband aliasing insertion.

6 Nearly Perfect Reconstruction DFT Modulated Filter Banks

So far perfect reconstruction subband systems were discussed. Perfect reconstruction ensures that signals are passed through the subband system without any quality losses. This perfect reconstruction property does not necessarily hold anymore when intermediate operations are performed on the subband signals (coding, filtering, ...). Furthermore, in practice the perfect reconstruction property is often overruled by non–linearities (e.g. AD–converters, loudspeakers), injected noise and algorithmic imperfections (residual errors for instance in the case of adaptive filtering). Perfect reconstruction can therefore be relaxed to 'nearly' perfect reconstruction by admitting some amplitude, phase and aliasing distortion as long as the distortion is not noticeable or is acceptably low. It depends on the application how far this nearly perfection can divert from the ideal, perfect reconstruction case.

One of the disadvantages of perfect reconstruction filter banks is that the subband filters typically have a non–negligible stopband level. In this way a considerable amount of aliasing is inserted in the subbands, which could have an impeding effect on the intermediate operations. A nearly perfect reconstruction filter bank could therefore be more appropriate and lead to better perceptual results : a better filter bank characteristic and hence reduced aliasing levels lead to a better performance of the intermediate algorithm (in the case of subband adaptive filtering for instance, as will be illustrated in section 7). Furthermore, in the approach taken in section 5 the analysis and the synthesis bank always have the same frequency characteristics. On the other hand, it is easy to design nearly perfect reconstruction systems for which the analysis and the synthesis filter bank characteristics are different or the order of the filter banks is not the same. Both a frequency–domain and a time–domain based optimisation algorithm were developed to design nearly perfect reconstruction subband systems.

6.1 Frequency–domain optimisation

For designing a nearly perfect reconstruction modulated filter bank set the lowpass properties of the analysis and/or synthesis prototype on the one hand and the overall amplitude distortion on the other hand can be optimised and traded off. Amplitude distortion is minimised instead of checking the true perfect reconstruction condition in order to reduce the computational load of the optimisation procedure. In some applications phase distortion is not detrimental as long as abrupt phase transitions are avoided. Small amplitude distortion will not cause significant quality losses. Instead of the overall amplitude distortion only the distortion from neighbouring bands is minimised in practice. The cost function to be optimised may be defined as

$$\int_{\frac{1}{2N}}^{\frac{1}{2}} (\alpha|H_0(f)| + \beta|G_0(f)|)df + \sqrt{\int_0^{\frac{1}{M}} \left(|H_0(f)G_0(f) + H_1(f)G_1(f)|^2 - N^2\right)^2 df}. \tag{41}$$

$H_0(f)$ and $G_0(f)$ are the frequency responses of respectively the analysis and the synthesis prototype, $H_1(f)$ and $G_1(f)$ are shifted versions of the prototypes and filter out the first frequency band as in figure 1. Finally α and β are weighting factors. The first term weights the stopband level of the analysis and synthesis prototype. The second term computes the amplitude distortion. Aliasing and phase distortion and the effect of the downsampling are not taken into account. The factor N^2 in Eq. 41 ensures that the input–output gain approaches 1 when the subband signals are N–fold downsampled.
Starting from a perfect reconstruction filter bank set (designed e.g. based on the procedure of section 5), one may want to relax the perfect reconstruction condition and enhance for instance the stopband level of the analysis prototype by minimising Eq. 41. Another starting point might be a filter bank set, based on an analysis and/or synthesis prototype with a sufficiently low stopband level obtained from a standard filter design tool, not fulfilling the perfect reconstruction condition. In that case one may approach perfect reconstruction

by changing the prototypes and minimising the amplitude distortion.
An **example** of a subband filter bank set, designed using this frequency–domain optimisation approach can be found in figure 7. The subband system has 8 subbands, which are 6–fold downsampled. The analysis and synthesis bank char-

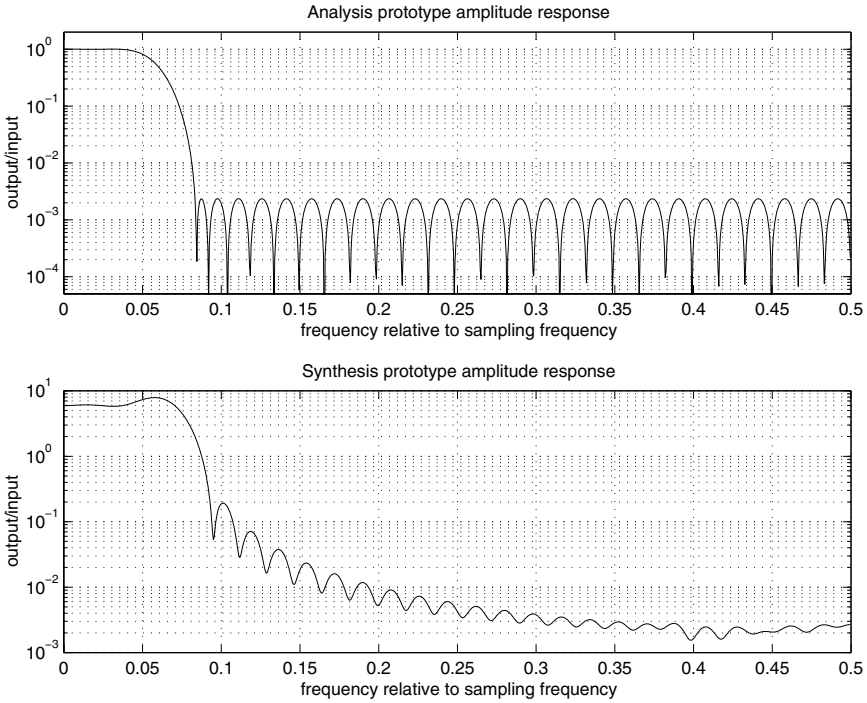

Figure 7: 8–subband 6–fold downsampled nearly perfect reconstruction filter bank set obtained by frequency–domain optimisation : prototype frequency characteristics

acteristics are different. The 60–taps analysis prototype was designed with the Parks–McClellan exchange algorithm and has a uniform stopband attenuation. The synthesis filter has 54 taps and was optimised following Eq. 41. The relative aliasing level (Eq. 40) introduced by the analysis bank is around -46.7 dB. The relative aliasing level of the synthesis bank prototype is -23.5 dB. The maximum amplitude distortion of the analysis–synthesis pair is 4.17 % at 0.45 Hz and the maximum phase distortion is 16° at 0.09 Hz. The subband system was tested for audio processing. The perceptual distortion was verified to be sufficiently small.
In a second example a 6–subband, 4–fold downsampled subband system was designed. The frequency characteristics of the analysis and synthesis prototype are shown in figure 8 (compare with figure 6) Both the analysis and synthesis prototype have 36 filter taps. The analysis prototype was designed with the

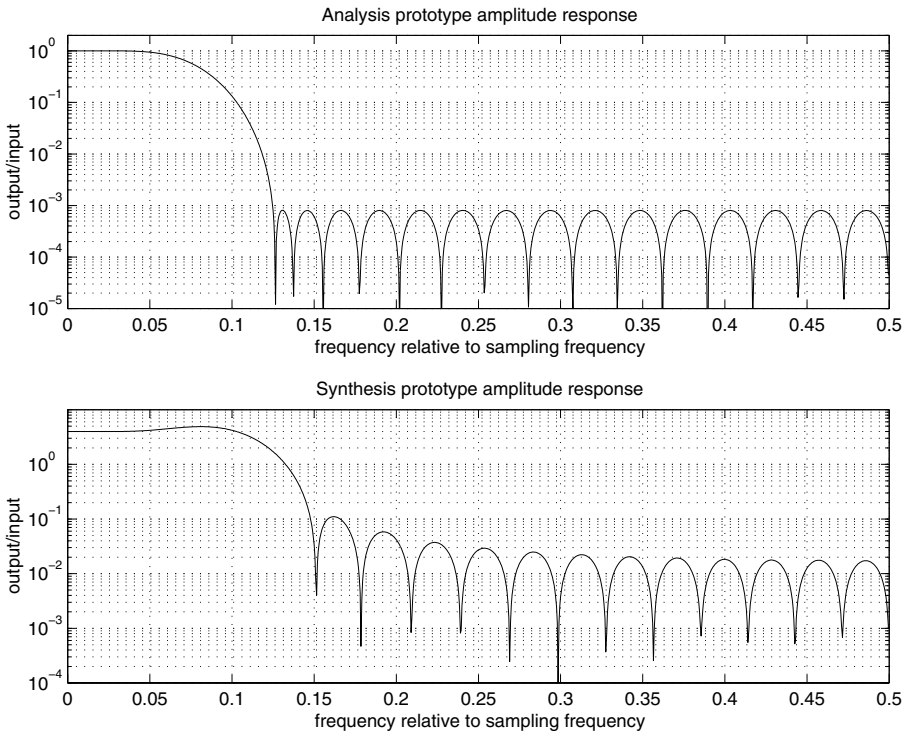

Figure 8: 6–subband 4–fold downsampled nearly perfect reconstruction filter bank set obtained by frequency–domain optimisation : prototype frequency characteristics

Parks–McClellan exchange algorithm. The relative aliasing level (Eq. 40) introduced by the analysis bank is -57.6 dB. The relative aliasing level of the synthesis bank is -20.3 dB. The maximum amplitude distortion of the analysis–synthesis pair is 0.21 % at 0.25 Hz and the maximum phase distortion is 0.0018° at 0.352 Hz. It was verified that the perceptual distortion is sufficiently small.

6.2 Time–domain optimisation

Another approach leading to nearly perfect reconstruction systems builds on the relation between the subband signals and the analysis bank input in the time domain. A similar approach was found in [1]. The input samples $x[k]$ are put

in an infinitely long vector $\mathbf{x}$ in the following way :

$$\mathbf{x} = \begin{bmatrix} \vdots \\ x[k-1] \\ x[k] \\ x[k+1] \\ \vdots \end{bmatrix} \tag{42}$$

The downsampled subband samples $x_m[n] = x_m[kN]$ for $m = 0 : M-1$ (see also figure 2) can be put in vector $\mathbf{s}$:

$$\mathbf{s} = \begin{bmatrix} \vdots \\ x_{M-1}[n-1] \\ x_0[n] \\ \vdots \\ x_{M-1}[n] \\ x_0[n+1] \\ \vdots \end{bmatrix}. \tag{43}$$

The relation between $\mathbf{x}$ and $\mathbf{s}$ can be expressed as

$$\mathbf{s} = \bar{\mathbf{T}}_H \mathbf{x}, \tag{44}$$

in which matrix $\bar{\mathbf{T}}_H$ has a band diagonal structure[4] and takes on the form shown in figure 9.

$\bar{\mathbf{T}}_H =$

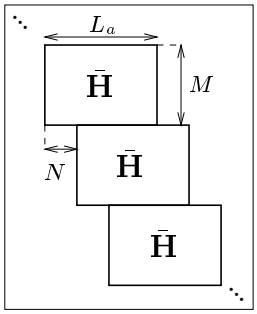

Figure 9: $\bar{\mathbf{T}}_H$ visualised

$\bar{\mathbf{H}}$ contains the analysis filter bank coefficients :

$$\bar{\mathbf{H}} = \begin{bmatrix} h_0[L_a-1] & \dots & h_0[0] \\ h_1[L_a-1] & \dots & h_1[0] \\ \vdots & \ddots & \vdots \\ h_{M-1}[L_a-1] & \dots & h_{M-1}[0] \end{bmatrix}. \tag{45}$$

[4]The bar indicates that the elements appear in time–reversed order.

If $L_a = PN$, with $P \in \mathbb{N}$, the analysis filters can be partitioned in P blocks as shown in figure 10.

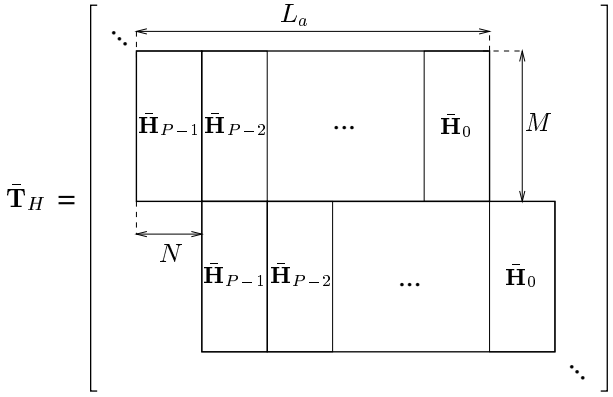

Figure 10: Block partitioning $\bar{\mathbf{T}}_H$

Similar expressions can be given for the synthesis part. An output vector $\mathbf{y}$

$$\mathbf{y} = \begin{bmatrix} \vdots \\ y[k-1] \\ y[k] \\ y[k+1] \\ \vdots \end{bmatrix} \tag{46}$$

and a synthesis matrix $\mathbf{T}_G$, again having a band diagonal structure containing matrix

$$\mathbf{G} = \begin{bmatrix} g_0[0] & \dots & g_0[L_a-1] \\ g_1[0] & \dots & g_1[L_a-1] \\ \vdots & \ddots & \vdots \\ g_{M-1}[0] & \dots & g_{M-1}[L_a-1] \end{bmatrix} \tag{47}$$

with the synthesis filters, are defined such that

$$\mathbf{y} = \mathbf{T}_G^T \mathbf{s}. \tag{48}$$

For the sake of conciseness, the analysis and synthesis filters are assumed to have equal length[5]. Partitioning $\mathbf{T}_G$ in the same way as $\mathbf{T}_H$, using blocks $\mathbf{G}_p$, leads to figure 11.

The perfect reconstruction properties follow from the inner matrix product $\mathbf{T}_G^T \bar{\mathbf{T}}_H$. Taking into account the filter partitioning, $\mathbf{T}_G^T \bar{\mathbf{T}}_H$ can be computed based on the block convolution of

$$\mathbf{V} = \begin{bmatrix} \mathbf{G}_0^T & \mathbf{G}_1^T & \dots & \mathbf{G}_{P-1}^T \end{bmatrix} \star \begin{bmatrix} \bar{\mathbf{H}}_0 & \bar{\mathbf{H}}_1 & \dots & \bar{\mathbf{H}}_{P-1} \end{bmatrix} \tag{49}$$

[5]If not, $\mathbf{H}$ or $\mathbf{G}$ should be padded with zeros.

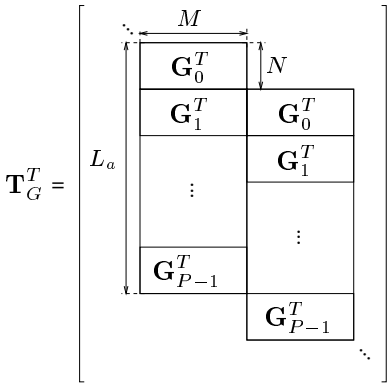

Figure 11: Block partitioning $\mathbf{T}_G^T$

i.e. (taking $\mathbf{H}_p = \mathbf{G}_p = 0$, if $p < 0$ or $p \geqslant P$)

$$\mathbf{V}_q = \sum_{p=0}^{P-1} \mathbf{G}_{P-1-p}^T \bar{\mathbf{H}}_{p+q}. \tag{50}$$

Perfect reconstruction implies

$$\mathbf{V}_0 = \mathbf{I}_N \tag{51}$$

$$\mathbf{V}_q = \mathbf{0}, \qquad \forall q \neq 0 \tag{52}$$

In the case of a para–unitary DFT modulated filter bank for which $L_a = PN$, Eq. 15, 16, 20 and 21 hold. It can be proven (see appendix B) that Eq. 51 and 52 are fulfilled in this case.
A filter bank can be designed that optimally meets conditions 51 and 52. A trade–off between these conditions and the lowpass properties of the analysis and/or the synthesis prototype filter should lead to a nearly perfect reconstruction subband system with a good stopband rejection. The cost function to be optimised may be defined as

$$\int_{\frac{1}{2N}}^{\frac{1}{2}} (\alpha |H_0(f)| + \beta |G_0(f)|) df + \left\| \begin{matrix} \mathbf{W}_{-P+1} \\ \vdots \\ \mathbf{W}_{P-1} \end{matrix} \right\|, \tag{53}$$

with $\mathbf{W}_0 = \mathbf{V}_0 - \mathbf{I}_N$ and $\mathbf{W}_q = \mathbf{V}_q$ if $q \neq 0$. Finally, α and β are weighting factors taking into account the stopband level of the analysis and synthesis prototype filter.
Example : figure 12 (compare with figure 6 and 8) shows again the analysis and synthesis prototype filters for a 6–subband, 4–fold downsampled subband system. Both the analysis and synthesis prototype have 36 filter taps. The

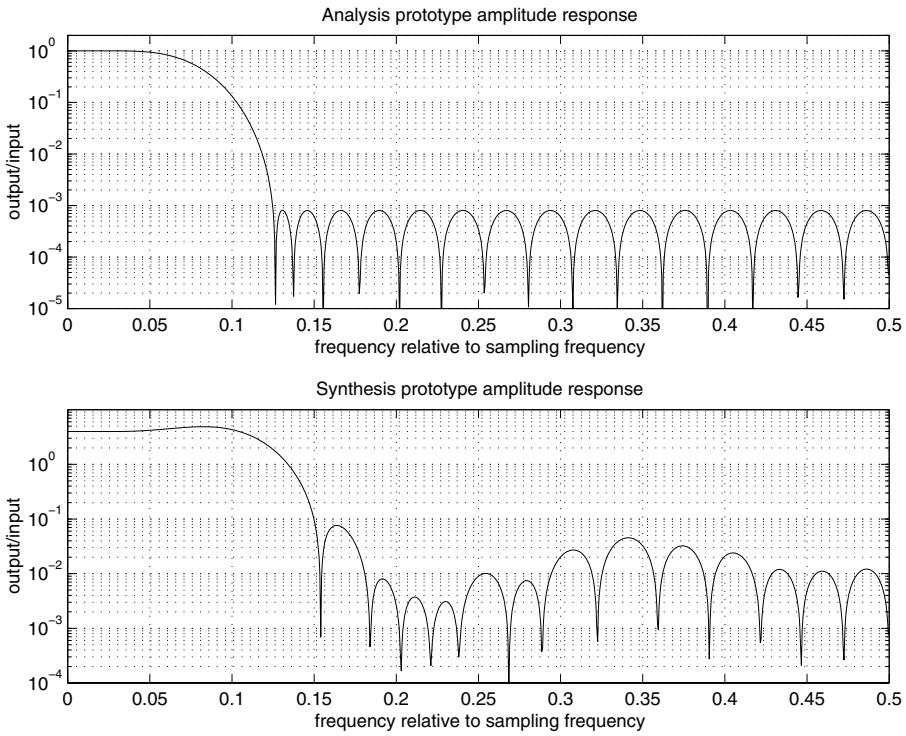

Figure 12: 6–subband 4–fold downsampled nearly perfect reconstruction filter bank set obtained by time–domain optimisation : prototype frequency characteristics

analysis prototype was designed with the Parks–McClellan exchange algorithm and is the same as in figure 8. The relative aliasing level (Eq. 40) introduced by the analysis bank is -57.6 dB. The relative aliasing level of the synthesis bank is -19.4 dB. The maximum amplitude distortion of the analysis–synthesis pair is 0.38 % at 0.211 Hz and the maximum phase distortion is 0.0023° at 0.319 Hz. The perceptual distortion was verified to be sufficiently small.

7 Application

One of the disadvantages of perfect reconstruction filter bank design is that the stopband level of the analysis prototype filter is difficult to control and to reduce to a sufficiently low level. Nearly perfect reconstruction systems offer more design freedom. As a result, it is easier to design and to specify the filter bank characteristics. In this way the amount of aliasing inserted in the subbands for instance can be kept small. This could have a positive impact on the operations performed on the subband signals, as will be illustrated in this section, taking

subband adaptive filtering as an example.
The general setup for a subband adaptive system is shown in figure 13. Both the

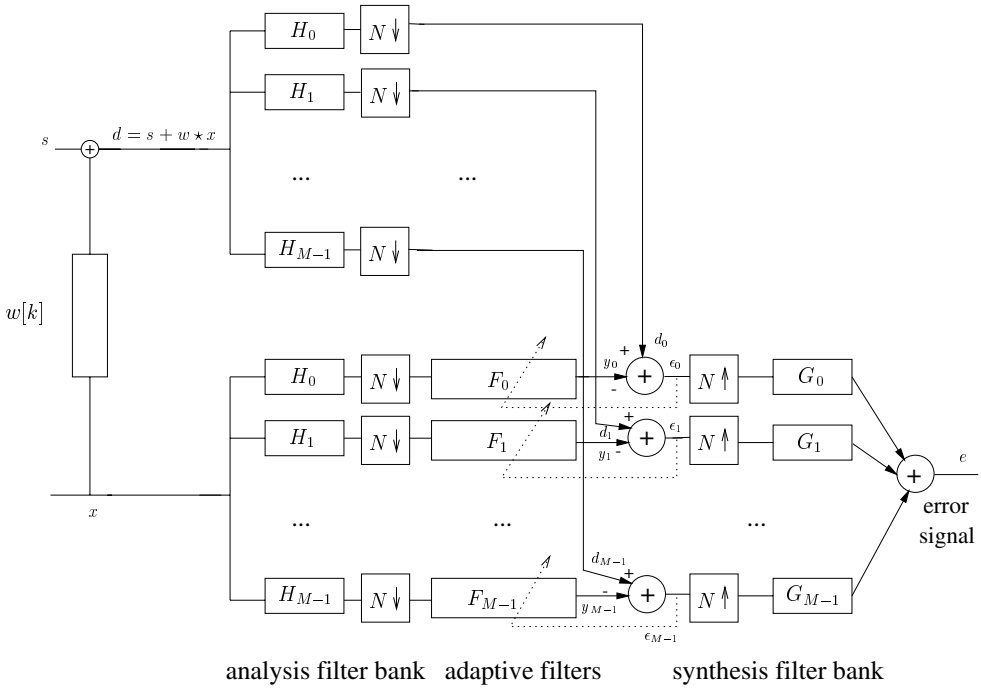

Figure 13: Subband adaptive filter setup : $w \star x$ needs to be suppressed and a non–distorted version of s has to be retained at the output e.

input signals x and d are fed into identical M–band analysis filter banks, with d being a filtered version of x by the unknown system $w[k]$. In most applications a so–called near–end signal s is added to $w \star x$ such that $d = s + w \star x$. After N–fold subsampling, adaptive filtering is done in each subband. The outputs of the subband adaptive filters are recombined in the synthesis filter bank leading to the final output. The ultimate goal is to suppress $w \star x$ at the output e and retaining a non–distorted version of s. Therefore, $w[k]$ is estimated using the set of parallel adaptive filters. This can be done by minimising the energy of the error output e. By splitting signals into subbands and subsequent subsampling faster (initial) convergence and better tracking properties are hoped for. A second advantage of subband systems over classical fullband adaptation is the lower achievable implementation cost (due to the downsampling). Also signal s is filtered and downsampled by the subband system. To minimise the distortion of s (nearly) perfect reconstruction filter banks are called for.
An experiment was carried out in which a Gaussian white noise signal was fed through a random 60–taps linear FIR filter w. There was no near–end signal

s added to d in this experiment. A subband setup as shown in figure 13 was used to estimate the unknown w. In this example $M = 6$, $N = 4$. In a first simulation the perfect reconstruction DFT modulated filter bank set of order 35 which was described in section 5.5 and figure 6 was used. The adaptive filters each had length 25. The error output of the algorithm is plotted in figure 14. Apparently some residual error remains, which is a phenomenon well known

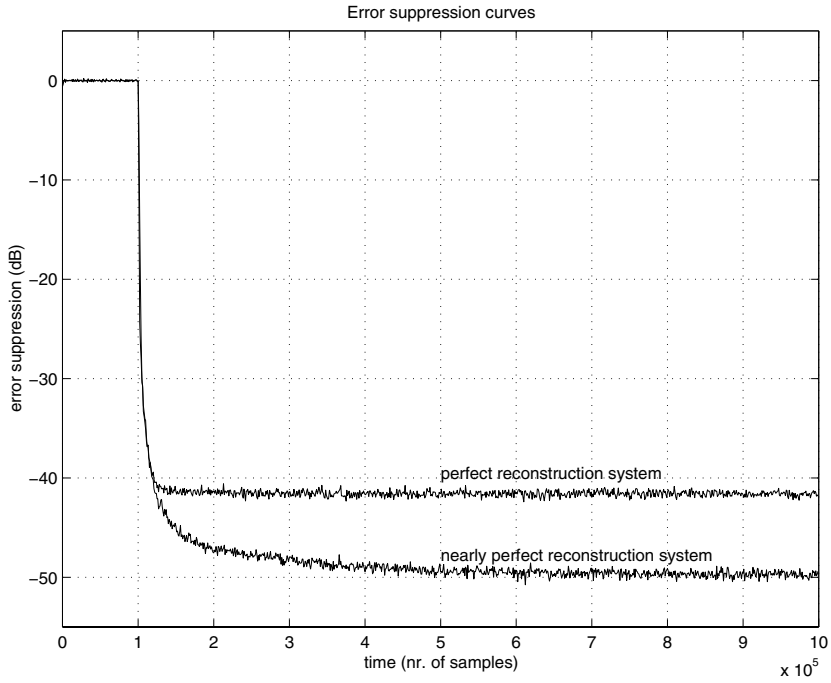

Figure 14: Simulation example : convergence curves for 2 subband adaptive systems, one based on a perfect reconstruction filter bank set, the other on nearly perfect reconstruction filter banks

from literature [5] and has to do with an undermodelling problem and injected subband aliasing. In a second simulation the nearly perfect reconstruction filter banks, obtained by the frequency–domain and time–domain optimisation procedure of section 6.1 and 6.2 (see also figure 8 and 12), were applied. The order of the filter banks and the length of the adaptive filters were the same as in the first simulation. As the characteristics of the time–domain and frequency–domain based filter banks are similar, the error curves lie almost on top of each other. Hence, only the error curve corresponding to the time–domain based filter bank set is shown in figure 14. It appears that although the maximum convergence rate which can be reached may be somewhat slower, a lower error energy and hence a better modelling can be achieved with the nearly perfect reconstruction system. Apparently the reduced stopband level of the nearly

perfect reconstruction filter banks leads to a better modelling of the unknown system. The number of perfect reconstruction filter bank coefficients equal to 0 is small in this example. Hence, a perfect reconstruction filter bank with a relatively good stopband attenuation could be designed (see also section 5.5). For other effective filter lengths, more coefficients need to be fixed to 0, leading to worse filter bank characteristics and higher aliasing levels. In that case the nearly perfect reconstruction systems would easily outperform their perfect reconstruction counterpart in this experiment. This example proves that thanks to their better filter bank characteristics nearly perfect reconstruction filter banks can outperform perfect reconstruction systems without introducing unacceptable audible distortion.

8 Conclusions

In this paper we have presented a design procedure for perfect reconstruction and nearly perfect reconstruction oversampled DFT modulated filter banks. A DFT modulated analysis/synthesis filter bank set is designed such that the output is an (almost perfect) delayed copy of the input ((nearly) perfect reconstruction) and the (analysis) filters are frequency selective. This last condition prevents inserting too much inter–subband aliasing during the downsampling operation. Inter–subband aliasing has a negative impact on possible intermediate operations performed on the subband signals (adaptive filtering for instance).
By exploiting the structure of the oversampled DFT modulated filter bank a para–unitary condition can be imposed, which guarantees perfect reconstruction. An algorithm was presented that optimises the lowpass characteristic of the filter banks leading to a perfect reconstruction subband system with minimal aliasing insertion.
Perfect reconstruction is a noble property, but often in practice it is overruled by the effect of the intermediate subband operations. By relaxing the perfect reconstruction property to nearly perfect reconstruction a subband system can be obtained with better frequency characteristics and hence reduced aliasing levels, leading to a better performance of the intermediate algorithms. Both a frequency–domain and time–domain based optimisation algorithm were developed to design nearly perfect reconstruction subband systems. Subband adaptive filtering was taken as an example to illustrate and compare the different design techniques.

9 Acknowledgements

Marc Moonen is a Research Associate with the F.W.O. (Fund for Scientific Research – Flanders). This research work was carried out at the ESAT laboratory of the Katholieke Universiteit Leuven, in the frame of the Belgian State Interuniversity Poles of Attraction Programme – IUAP P4–02 (1997–2001) : Modeling, Identification, Simulation and Control of Complex Systems, Concerted

Research Action GOA–MEFISTO–666 of the Flemish Government, Research Project F.W.O. nr. G.0295.97 ('Design and implementation of adaptive digital signal processing algorithms for broadband applications') and IWT project AUT/970517: MUSETTE ('Multimicrophone Signal Enhancement Techniques for handsfree telephony and voice controlled systems'). The scientific responsibility is assumed by its authors.

References

[1] A. Akansu and M. Smith. *Subband and Wavelet Transforms.* Kluwer Academic Publishers, Boston, 1995.

[2] Z. Cvetković. Oversampled Modulated Filter Banks and Tight Gabor Frames in $l^2(\mathbb{Z})$. In *Proceedings of the 1995 IEEE Int. Conf. on Acoust., Speech and Signal Processing*, pages 1456–1459, Detroit, Michigan, USA, May 1995.

[3] K. Eneman and M. Moonen. Para-Unitary Filter Bank Design for Oversampled Subband Systems. Technical Report 97-119, ESAT–SISTA, Katholieke Universiteit Leuven, Belgium, December 1997.

[4] K. Eneman and M. Moonen. DFT Modulated Filter Bank Design for Oversampled Subband Systems. In *Proceedings of the IEEE Benelux Signal Processing Symposium*, pages 87–90, Leuven, Belgium, March 1998.

[5] K. Eneman and M. Moonen. Hybrid Subband/Frequency–Domain Adaptive Systems. *Signal Processing*, 81(1):117–136, January 2001.

[6] M. Harteneck, R. Stewart, and J. Páez-Borrallo. A Filterbank Design for Oversampled Filter Banks without Aliasing in the Subbands. In *Proceedings of the 2nd UK Symposium on Applications of Time-Frequency and Time-Scale Models (TFTS97)*, pages 161–164, Warwick, UK, August 1997.

[7] N. Jayant, J. Johnston, and R. Safranek. Signal Compression Based on Models of Human Perception. *Proceeding of the IEEE*, 81(10):1385–1421, October 1993.

[8] K. Kajita, H. Kobayashi, S. Muramatsu, A. Yamada, and H. Kiya. A Design Method for Oversampled Paraunitary DFT Filter Banks using Householder Factorization. In *Proceedings of the European Signal Processing Conference (EUSIPCO-96)*, pages 192–195, Trieste, Italy, September 1996.

[9] J. Shynk. Frequency-Domain and Multirate Adaptive Filtering. *IEEE Signal Processing Magazine*, 9(1):15–37, January 1992.

[10] P. Vaidyanathan. *Multirate Systems and Filter Banks.* Prentice Hall, Englewood Cliffs, New Jersey, USA, 1993.

[11] M. Vetterli and Z. Cvetković. Oversampled FIR Filter Banks and Frames in $l^2(\mathbb{Z})$. In *Proceedings of the 1996 IEEE Int. Conf. on Acoust., Speech and Signal Processing*, pages 1530–1533, Atlanta, Georgia, USA, May 1996.

[12] M. Vetterli and J. Kovačević. *Wavelets and Subband Coding.* Prentice Hall, Englewood Cliffs, New Jersey, USA, 1995.

[13] M. Vetterli and D. Le Gall. Perfect Reconstruction FIR Filter Banks: Some Properties and Factorizations. *IEEE Trans. Acoust., Speech and Signal Processing*, 37(7):1057–1071, July 1989.

[14] X.-G. Xia and B. Suter. FIR Paraunitary Filter Banks Given Several Analysis Filters: Factorizations and Constructions. *IEEE Trans. Signal Processing*, 44(3):720–723, March 1996.

A Inverse decomposition of para–unitary lattices

Whereas in the decomposition problem (Eq. 28) $\mathbf{M}_\gamma(z)$ is parametrised such that the underlying filter bank is para–unitary, inverse decomposition deals with finding the unit–norm vectors $\mathbf{v}_i$ and $\mathbf{u}_i$ for a given $\mathbf{M}_\gamma(z)$.
The polyphase components of the prototype filter of a para–unitary filter bank can be put into sub–matrices $\hat{\mathbf{S}}_\gamma(z)$ (Eq. 26). Now, if $M > N$ each of the para–unitary submatrices $\hat{\mathbf{S}}_\gamma(z)$ is rectangular and is embedded in a larger square $\frac{M}{g} \times \frac{M}{g}$ matrix $\mathbf{M}_\gamma(z)$. We repeat formula 28 :

$$\mathbf{M}_\gamma^{(L)}(z) = \mathbf{V}_L(z)\mathbf{V}_{L-1}(z)\ldots\mathbf{V}_1(z)\mathbf{U}. \tag{54}$$

$\mathbf{V}_i(z)$ are degree–1 para–unitary building blocks :

$$\mathbf{V}_i(z) = \mathbf{I} - \mathbf{v}_i\mathbf{v}_i^T + z^{-1}\mathbf{v}_i\mathbf{v}_i^T \tag{55}$$

and $\mathbf{U}^T\mathbf{U} = \mathbf{I}$. Further, $\mathbf{v}_i$ are $\frac{M}{g} \times 1$ column vectors having unit norm.
So,

$$\hat{\mathbf{S}}_\gamma(z) = \bar{\mathbf{M}}_\gamma^{(L)}(z) = \mathbf{V}_L(z)\mathbf{V}_{L-1}(z)\ldots\mathbf{V}_1(z)\mathbf{U}|_{1:N/g} \tag{56}$$

in which $\mathbf{U}|_{1:N/g}$ contains the first $\frac{N}{g}$ columns of $\mathbf{U}$. Introducing $\bar{\mathbf{M}}_\gamma^{(L-1)}(z)$:

$$\bar{\mathbf{M}}_\gamma^{(L-1)}(z) = \mathbf{V}_{L-1}(z)\ldots\mathbf{V}_1(z)\mathbf{U}|_{1:N/g} \tag{57}$$

it appears that

$$\bar{\mathbf{M}}_\gamma^{(L)}(z) = \mathbf{V}_L(z)\bar{\mathbf{M}}_\gamma^{(L-1)}(z). \tag{58}$$

The z^{-L}–part of $\bar{\mathbf{M}}_\gamma^{(L)}(z)$ is (see Eq. 55)

$$\mathbf{v}_L\mathbf{v}_L^T\cdot\left(z^{-(L-1)}\text{–part of }\bar{\mathbf{M}}_\gamma^{(L-1)}(z)\right) \tag{59}$$

which is a rank–1 matrix. $\mathbf{v}_L$ can therefore be found as the first left singular vector of the z^{-L}–part of $\bar{\mathbf{M}}_\gamma^{(L)}(z)$. The next step will be the recovery of $\bar{\mathbf{M}}_\gamma^{(L-1)}(z)$.

Consider the general case where $\mathbf{v}_i$ and $\bar{\mathbf{M}}_\gamma^{(i)}(z)$ are known and $\bar{\mathbf{M}}_\gamma^{(i-1)}(z)$ needs to be found. Define $\mathbf{A}_i = \mathbf{I} - \mathbf{v}_i\mathbf{v}_i^T$ and $\mathbf{B}_i = \mathbf{v}_i\mathbf{v}_i^T$. Now from Eq. 55,

$$\bar{\mathbf{M}}_\gamma^{(i)}(z) = (\mathbf{A}_i + z^{-1}\mathbf{B}_i)\bar{\mathbf{M}}_\gamma^{(i-1)}(z). \tag{60}$$

Define

$$\bar{\mathbf{M}}_\gamma^{(i)}(z) = \sum_{k=0}^{i} \bar{\mathbf{H}}_i^{(k)} z^{-k} \tag{61}$$

then

$$\sum_{k=0}^{i} \bar{\mathbf{H}}_i^{(k)} z^{-k} = (\mathbf{A}_i + z^{-1}\mathbf{B}_i) \sum_{k=0}^{i-1} \bar{\mathbf{H}}_{i-1}^{(k)} z^{-k}. \tag{62}$$

If it is assumed that $\bar{\mathbf{H}}_i^{(k)} = 0$ if $k < 0$ or $k > i$, then

$$\bar{\mathbf{H}}_i^{(k)} = \mathbf{A}_i\bar{\mathbf{H}}_{i-1}^{(k)} + \mathbf{B}_i\bar{\mathbf{H}}_{i-1}^{(k-1)}, \quad \forall k. \tag{63}$$

This leads to the following set of linear equations :

$$\begin{bmatrix} \bar{\mathbf{H}}_i^{(0)} \\ \bar{\mathbf{H}}_i^{(1)} \\ \vdots \\ \bar{\mathbf{H}}_i^{(i-1)} \\ \bar{\mathbf{H}}_i^{(i)} \end{bmatrix} = \begin{bmatrix} \mathbf{A}_i & \mathbf{0} & \dots & \mathbf{0} \\ \mathbf{B}_i & \mathbf{A}_i & \dots & \mathbf{0} \\ \vdots & \vdots & \ddots & \vdots \\ \mathbf{0} & \mathbf{0} & \dots & \mathbf{A}_i \\ \mathbf{0} & \mathbf{0} & \dots & \mathbf{B}_i \end{bmatrix} \begin{bmatrix} \bar{\mathbf{H}}_{i-1}^{(0)} \\ \bar{\mathbf{H}}_{i-1}^{(1)} \\ \vdots \\ \bar{\mathbf{H}}_{i-1}^{(i-1)} \end{bmatrix}. \tag{64}$$

$\bar{\mathbf{M}}_\gamma^{(i-1)}(z)$ can therefore be found based on $\bar{\mathbf{M}}_\gamma^{(i)}(z)$ and the pseudo–inverse of the double block diagonal matrix in the previous equation. $\mathbf{v}_{i-1}$ is again found as the first left singular vector of the $z^{-(i-1)}$–part of $\bar{\mathbf{M}}_\gamma^{(i-1)}(z)$. This procedure can be repeated until a zero–order rectangular $\bar{\mathbf{M}}_\gamma^{(0)}(z)$ remains. However, a square orthonormal matrix $\mathbf{U}$ is needed to compute the $\mathbf{u}_i$'s. By QR–decomposition of $\bar{\mathbf{M}}_\gamma^{(0)}(z)$ a set of $\frac{M}{g} - \frac{N}{g}$ column vectors can be obtained which are orthogonal to $\bar{\mathbf{M}}_\gamma^{(0)}(z)$. They serve as the $\frac{M}{g} - \frac{N}{g}$ missing columns to form the orthonormal $\mathbf{U}$. The decomposition of $\mathbf{U}$ is based on its Householder factorisation :

$$\mathbf{U} = \mathbf{U}_1\mathbf{U}_2 \dots \mathbf{U}_{M/g-1}. \tag{65}$$

$\mathbf{U}_i$ are Householder matrices : $\mathbf{U}_i = \mathbf{I} - 2\mathbf{u}_i\mathbf{u}_i^T$ in which $\mathbf{u}_i$ are $\frac{M}{g} \times 1$ column vectors having unit norm. They can be contained in a description matrix having the special format given in Eq. 32.

It can be proven (see [10]) that there exists a unit–norm vector $\mathbf{u}_1$ such that

$$\mathbf{U}_1\mathbf{U} = (\mathbf{I} - 2\mathbf{u}_1\mathbf{u}_1^T)\mathbf{U} = \begin{bmatrix} 1 & \mathbf{0} \\ \mathbf{0} & \mathbf{T}_1 \end{bmatrix}, \qquad \mathbf{T}_1^T\mathbf{T}_1 = \mathbf{I}. \tag{66}$$

So, with $\mathbf{U}|_1$ defined as the first column of $\mathbf{U}$,

$$-2\mathbf{u}_1\mathbf{u}_1^T\mathbf{U}|_1 = \begin{bmatrix} 1 \\ \mathbf{0} \end{bmatrix} - \mathbf{U}|_1. \tag{67}$$

Normalising both sides

$$\frac{-2\mathbf{u}_1\mathbf{u}_1^T\mathbf{U}|_1}{\sqrt{4\mathbf{U}|_1^T\mathbf{u}_1\mathbf{u}_1^T\mathbf{u}_1\mathbf{u}_1^T\mathbf{U}|_1}} = \frac{\begin{bmatrix} 1 \\ \mathbf{0} \end{bmatrix} - \mathbf{U}|_1}{\left\|\begin{bmatrix} 1 \\ \mathbf{0} \end{bmatrix} - \mathbf{U}|_1\right\|} \tag{68}$$

and taking in account that $\mathbf{u}_1^T\mathbf{u}_1 = 1$ and $\mathbf{U}|_1^T\mathbf{u}_1$ is a scalar, we obtain

$$\mathbf{u}_1 = -\frac{\begin{bmatrix} 1 \\ \mathbf{0} \end{bmatrix} - \mathbf{U}|_1}{\left\|\begin{bmatrix} 1 \\ \mathbf{0} \end{bmatrix} - \mathbf{U}|_1\right\|}. \tag{69}$$

From Eq. 66 an orthonormal $\mathbf{T}_1$ can now be computed. Applying Eq. 66 and 69 recursively to $\mathbf{T}_1$ leads to $\mathbf{u}_2$. $\mathbf{T}_2$ can be computed from $\mathbf{T}_1$ and $\mathbf{u}_2$ using Eq. 66. This procedure can be further recursively applied to obtain $\mathbf{u}_3, \ldots, \mathbf{u}_{M/g-1}$.

B Time–domain optimised nearly perfect reconstruction systems : special case of para–unitary DFT modulated filter banks

In this appendix we will prove that a para–unitary DFT modulated filter bank as described by Eq. 15, 16, 20 and 21 fulfils the perfect reconstruction conditions presented in Eq. 51 and 52.
Based on Eq. 21 and the partitioning of $\mathbf{H}$ and $\mathbf{G}$ shown in figure 10 and 11, we obtain

$$\mathbf{H}_p = \begin{bmatrix} h_0[pN] & \ldots & h_0[pN+N-1] \\ \vdots & \ddots & \vdots \\ h_{M-1}[pN] & \ldots & h_{M-1}[pN+N-1] \end{bmatrix} \tag{70}$$

$$\mathbf{G}_p = \frac{1}{M}\bar{\mathbf{H}}_{P-1-p}^* = \frac{1}{M}\mathbf{H}_{P-1-p}^*\boldsymbol{J}. \tag{71}$$

For this we can compute

$$\mathbf{V}_q = \sum_{p=0}^{P-1}\mathbf{G}_{P-1-p}^T\bar{\mathbf{H}}_{p+q} = \frac{1}{M}\sum_{p=0}^{P-1}\boldsymbol{J}\mathbf{H}_p^{*T}\mathbf{H}_{p+q}\boldsymbol{J} \tag{72}$$

which should be unity for $q = 0$ and zero elsewhere to ensure perfect reconstruction.

The perfect reconstruction property is fulfilled for an M–band, N–fold downsampled subband system if the analysis polyphase matrix $\mathbf{H}(z)$ is para–unitary, i.e. if

$$\tilde{\mathbf{H}}(z)\mathbf{H}(z) = \alpha \mathbf{I}_N. \tag{73}$$

α is an arbitrary number, different from 0. Further, we assume that $L_a = PN$ with $P \in \mathbb{N}$. In the case of a para–unitary DFT modulated filter bank for which $\mathbf{H}(z) = \mathbf{F}\mathbf{B}(z)$ and $\tilde{\mathbf{B}}(z)\mathbf{B}(z) = \mathbf{I}_N$ (cf. Eq. 20), it appears that $\alpha = M$. Now $\mathbf{H}(z)$ can be written as

$$\mathbf{H}(z) = \sum_{l=0}^{P-1} z^{-l}\mathbf{H}^{(l)}. \tag{74}$$

$\mathbf{H}^{(l)}$ is a matrix containing the l–th order coefficients of $\mathbf{H}(z)$. Element (m, n) of $\mathbf{H}^{(l)}$ therefore is

$$\left[\mathbf{H}^{(l)}\right]_{mn} = h_m[n + lN] \tag{75}$$

and hence $\mathbf{H}^{(l)}$ corresponds to $\mathbf{H}_l$ as defined in Eq. 70. So,

$$\mathbf{H}(z) = \sum_{l=0}^{P-1} z^{-l}\mathbf{H}_l. \tag{76}$$

$\tilde{\mathbf{H}}(z)\mathbf{H}(z) = M\mathbf{I}_N$ therefore implies

$$(\mathbf{H}_0^{*T} + z\mathbf{H}_1^{*T} + \cdots + z^{P-1}\mathbf{H}_{P-1}^{*T})(\mathbf{H}_0 + z^{-1}\mathbf{H}_1 + \cdots + z^{-(P-1)}\mathbf{H}_{P-1}) = M\mathbf{I}_N. \tag{77}$$

This is equivalent to

$$\frac{1}{M}\sum_{p=0}^{P-1} \mathbf{H}_p^{*T}\mathbf{H}_p = \mathbf{I}_N \qquad \text{term corresponding to } z^0 \tag{78}$$

$$\sum_{p=0}^{P-1} \mathbf{H}_p^{*T}\mathbf{H}_{p+q} = \mathbf{0}_N \qquad \text{terms corresponding to } z^{-q} \tag{79}$$

which is in accordance with Eq. 51, 52 and 72.